MNRAS 000, 1–9 () Preprint 3 March 2017 Compiled using MNRAS LATEX style file v3.0

# H I 21-cm absorption from $z \sim 0.35$ strong Mg II absorbers

R. Dutta[1]⋆, R. Srianand[1]†, N. Gupta[1]‡, R. Joshi[1]§
[1] *Inter-University Centre for Astronomy and Astrophysics, Post Bag 4, Ganeshkhind, Pune 411007, India*

arXiv:1703.00457v1 [astro-ph.GA] 1 Mar 2017

Accepted. Received; in original form

**ABSTRACT**

We have searched for H I 21-cm absorption in 11 strong Mg II systems ($W_{\rm r}$(Mg II $\lambda$2796) $\geqslant$ 1 Å) at $0.3 < z < 0.5$ using the Giant Metrewave Radio Telescope. We have detected H I 21-cm absorption in two of these. From the integrated optical depth ($\int \tau dv$) we estimate $N$(H I) = 43 $\pm$ 2 and 9 $\pm$ 2 in units of $10^{19}$ cm$^{-2}$ for the absorbers towards J1428+2103 ($z_{\rm abs}$ = 0.3940) and J1551+0713 ($z_{\rm abs}$ = 0.3289), respectively, assuming spin temperature, $T_{\rm s}$ = 100 K, and gas covering factor, $C_{\rm f}$ = 1. The velocity width of the H I absorption towards J1428+2103 and J1551+0713 indicate that the gas temperature is <1600 K and <350 K, respectively. The $3\sigma$ upper limits on $\int \tau dv$ in case of the H I 21-cm non-detections indicate that these Mg II absorbers are likely to arise from sub-damped Lyman-$\alpha$ systems, when we assume $T_{\rm s}$ = 100 K and $C_{\rm f}$ = 1. This is verified for one of the systems which has $N$(H I) measurement using Lyman-$\alpha$ absorption detected in the ultraviolet spectrum. We estimate the detection rate of H I 21-cm absorption in strong Mg II systems in our sample to be $0.18^{+0.24}_{-0.12}$ at $z \sim 0.35$, for an integrated optical depth sensitivity of $\leqslant$ 0.3 km s$^{-1}$. Comparing with the results of H I 21-cm absorption surveys in strong Mg II systems at higher redshifts from the literature, we do not find any significant evolution in the incidence and number density per unit redshift of H I 21-cm absorbers in strong Mg II systems over $0.3 < z < 1.5$.

**Key words:** galaxies: ISM – quasars: absorption lines.

## 1 INTRODUCTION

H I 21-cm absorption is an excellent tool to study the physical conditions of high column density cold (∼100 K) neutral gas in galaxies (Kulkarni & Heiles 1988). Studies of H I 21-cm absorption at different redshifts can be used to trace the redshift evolution of the cold gas fraction in galaxies, and hence understand the processes driving the observed redshift evolution of the global star formation rate density (SFRD; Madau & Dickinson 2014). There have been several H I 21-cm absorption searches towards radio-loud quasars that show intervening absorption in their optical or ultraviolet (UV) spectra (e.g. Briggs & Wolfe 1983; Lane 2000; Kanekar & Chengalur 2003; Curran et al. 2005; Gupta et al. 2009; Kanekar et al. 2009; Curran et al. 2010; Srianand et al. 2012; Gupta et al. 2012; Kanekar et al. 2014; Dutta et al. 2017b), or are at small impact parameters ($b$) from foreground galaxies (e.g. Carilli & van Gorkom 1992; Gupta et al. 2010, 2013; Borthakur et al. 2011; Borthakur 2016; Zwaan et al. 2015; Reeves et al. 2015, 2016; Dutta et al. 2016, 2017a). These studies have indicated that the distribution of cold H I gas around low-$z$ ($z < 0.4$) galaxies is patchy (see Srianand et al. 2013), with an average covering factor of ∼20% within $b$ ∼35 kpc (see Dutta et al. 2017a), and that the H I gas at high-$z$ ($z > 2$) is predominantly warmer (spin temperature, $T_{\rm s} \gtrsim$ 1000 K) compared to the Milky Way (see Srianand et al. 2012; Kanekar et al. 2014). However, careful mapping and interpretation of the redshift evolution of the cold gas fraction based on the present measurements is difficult due to different sample selection techniques used at different redshifts, and the small number of H I 21-cm detections known till date.

Strong Mg II absorbers [i.e. rest equivalent width (REW) of Mg II $\lambda$2796, $W_{\rm Mg\,II} \geqslant$ 1.0 Å] have been shown to be associated with galaxies (Bergeron 1986; Lanzetta & Bowen 1990; Bergeron & Boissé 1991; Steidel 1995; Guillemin & Bergeron 1997; Churchill et al. 2005; Chen et al. 2010; Rao et al. 2011; Bowen & Chelouche 2011), and trace gas with high $N$(H I) (Rao et al. 2006), like damped Lyman-$\alpha$ absorbers (DLAs) and sub-DLAs which have $N$(H I) $\geqslant 2\times10^{20}$ cm$^{-2}$ and $\sim 10^{19} - 2\times10^{20}$ cm$^{-2}$, respectively (see for a review Wolfe et al. 2005). Hence, they are appropriate targets to carry out H I 21-cm absorption searches, especially at $z < 1.5$ where ground-based observations of DLAs are limited by the atmospheric cutoff of light below 3000 Å. Large homogeneous samples of Mg II absorbers are available (e.g. Nestor et al. 2005; Prochter et al. 2006; Quider et al.

⋆ E-mail: rdutta@iucaa.in
† E-mail: anand@iucaa.in
‡ E-mail: ngupta@iucaa.in
§ E-mail: rjoshi@iucaa.in

© The Authors

2011; Zhu & Ménard 2013), thanks to the large database of quasar spectra in the Sloan Digital Sky Survey (SDSS; York et al. 2000). Taking advantage of this, there have been systematic searches for H I 21-cm absorption in SDSS-selected samples of Mg II systems at $0.5 < z < 1.5$ (Gupta et al. 2007, 2009, 2012; Kanekar et al. 2009; Dutta et al. 2017b). Gupta et al. (2012) have shown that the detection rate of H I 21-cm absorption in strong Mg II systems remains constant over this redshift range, within the uncertainties, which is intriguing given the proposed connection between redshift evolution of the global SFRD and strong Mg II absorption (e.g. Ménard et al. 2011; Chen et al. 2016). Dutta et al. (2017b) have shown that strong Mg II absorbers have higher probability being DLAs and giving rise to H I 21-cm absorption when strong Fe II absorption (REW of Fe II $\lambda$2600, $W_{\rm Fe\,II} \geqslant 1$ Å) is present. However, even the strong Fe II systems show no clear evolution in incidence of H I 21-cm absorption at $0.5 < z < 1.5$.

On the other hand, the incidence of H I 21-cm absorption in DLAs increases from $\sim$20% at $z > 2$ to $\sim$60% at $z < 1$ (Kanekar et al. 2009; Srianand et al. 2012; Dutta et al. 2017b). Further, the incidence of $H_2$ absorption in DLAs/sub-DLAs increases from $\sim$10% at $z \geqslant 1.8$ (Noterdaeme et al. 2008) to $\sim$50% at $z \leqslant 0.7$, with most of the $H_2$ absorption at low-$z$ arising from sub-DLAs at $b > 10$ kpc from the host galaxies (Muzahid et al. 2015). Hence, the physical conditions and origin of cold gas around galaxies could be significantly different at low-$z$. The lower redshift cutoff of the Mg II samples searched for H I 21-cm absorption has usually been chosen as $z \sim 0.5$ due to the difficulty of identifying large number of Mg II absorbers in the low signal-to-noise ratio (SNR) blue part of the SDSS spectra. Till date there have been only few searches for H I 21-cm absorption in strong Mg II selected systems at $z < 0.5$ (see Lane 2000, and references therein). Now due to the increased wavelength coverage and SNR of SDSS-Baryon Oscillation Spectroscopic Survey (BOSS) in the blue part, Mg II absorption can be searched upto $z = 0.3$ in the quasar spectra.

Here we wish to extend the H I 21-cm absorption studies in strong Mg II systems to lower redshifts (i.e. $z < 0.5$), in order to study the redshift evolution of incidence of H I 21-cm absorption in these systems. Additionally, it is relatively easier to identify and study the properties of host galaxies at these redshifts. Hence, this will allow us to connect between H I 21-cm studies in $0.5 < z < 1.5$ strong Mg II systems and $z < 0.4$ galaxy-selected samples. Further, due to the lack of a statistically significant DLA sample at low-$z$, the evolution of the cosmic H I mass density ($\Omega_{\rm H\,I}$) at $z < 1.5$ has been a matter of debate (e.g. Rao et al. 2006; Neeleman et al. 2016). Hence, studying how the incidence of cold H I gas evolves over this redshift range will help to shed light on the redshift evolution of $\Omega_{\rm H\,I}$.

We present here the results from our Giant Metrewave Radio Telescope (GMRT) search for H I 21-cm absorption in eleven strong Mg II systems at $0.3 < z < 0.5$ selected from SDSS. Our sample has increased the number of observed strong Mg II systems in this redshift range (see Lane 2000, for the previous compilation, and Section 5.1 for further details) by a factor of three. This paper is structured as follows. We describe our sample in Section 2 and our GMRT observations in Section 3. We present the results from our search for H I 21-cm absorption in Section 4. We discuss and summarize our results in Sections 5 and 6, respectively. Throughout this work we use a flat $\Lambda$-cold dark matter cosmology with $H_0 = 70\,{\rm km\,s^{-1}\,Mpc^{-1}}$ and $\Omega_{\rm M} = 0.30$.

## 2 SAMPLE SELECTION AND PROPERTIES

We identified 298 quasars from SDSS Data Release 12 (DR12; Alam et al. 2015) with: (a) peak flux density at 1.4 GHz $> 50$ mJy from the Faint Images of the Radio Sky at Twenty-Centimeters (FIRST; White et al. 1997) survey, to allow a sensitive search for H I 21-cm absorption; and (b) $z_{\rm em} < 1.95$, such that the Lyman-$\alpha$ forest is below 3600 Å (i.e. not covered by the SDSS spectra). In the SDSS spectra of these quasars, we visually searched for strong Mg II absorption ($W_{\rm Mg\,II} \geqslant 1.0$ Å) at $0.29 < z_{\rm abs} < 0.42$. We identified 12 such Mg II absorbers, which form the complete sample of strong Mg II-selected systems at these redshifts that can be searched for H I 21-cm absorption using L-band of GMRT. The details of these absorbers are presented in Table 1.

The median values of $W_{\rm Mg\,II}$ and the Mg II doublet ratio of the absorbers in our sample are 1.27 Å and 1.25, respectively. Mg I absorption is detected in 8 of these strong Mg II systems (though the Mg I absorption towards J1428+2103 could be blended with a metal line from another absorber), with a median $W_{\rm r}({\rm Mg\,I}\ \lambda2852)/W_{\rm Mg\,II} = 0.39$. Fe II absorption lines from the strong Mg II systems are not covered in the SDSS spectra, except for J1628+4734 [1]. In case of J1628+4734, absorption from Fe II $\lambda$2600 and $\lambda$2586 are not detected in the SDSS spectrum, and we estimate a $3\sigma$ upper limit of $W_{\rm Fe\,II} \leqslant 0.4$ Å. Note that the Mg II absorption towards J1628+4734 has a very broad profile and no other associated absorption is detected. The presence of Ca II and Na I absorption usually indicates that the gas has high $N$(H I). Ca II absorption is detected from the Mg II systems towards J1514+2813 (REW of Ca II $\lambda$3934, $W_{\rm Ca\,II} = 0.48 \pm 0.09$ Å), J1551+0713 ($W_{\rm Ca\,II} = 0.30 \pm 0.06$ Å), and J1619+3030 ($W_{\rm Ca\,II} = 0.27 \pm 0.07$ Å). Na I absorption is detected only from the Mg II system towards J1619+3030 (REW of Na I $\lambda$5891, $W_{\rm Na\,I} = 0.11 \pm 0.06$ Å).

In the SDSS images of all the quasars, we find at least one candidate host galaxy of the strong Mg II absorption at $b < 110$ kpc, which has photometric redshift consistent with the absorber redshift within the uncertainties (see Table 1). The SDSS $r$-band magnitude of the nearest host galaxy candidates are in the range of 20.2−22.2 with a median of 20.8, and their observed $g - r$ colours are in the range of 0.0−2.3 with a median of 1.1. The host galaxies could also be faint galaxies in proximity or superimposed to the bright quasars, and hence difficult to detect in the SDSS images. Nebular emission lines are usually detected in such cases of 'galaxy on top of quasars' (e.g. Noterdaeme et al. 2010; York et al. 2012; Straka et al. 2013). However, we do not detect any nebular emission lines at the redshift of the Mg II absorption in the SDSS spectra of the quasars. The non-detection of [O II] $\lambda$3727 emission at the redshift of the Mg II absorption in the median stacked spectrum of the quasars (after subtracting the quasar continuum) provides a $3\sigma$ upper limit on the average surface star formation rate density of $4 \times 10^{-4}\,{\rm M_\odot\,yr^{-1}\,kpc^{-2}}$ (following Kewley et al. 2004). Deep images and spectroscopic redshifts of all the galaxies in the field around the quasars are required to understand the origin of the strong Mg II absorbers.

Recently, it has been shown that the systems with H I 21-cm absorption cause systematic reddening in the spectrum of the background quasar (Dutta et al. 2017b). We estimate the redden-

[1] In case of J0209−0438 and J1608+1029, the expected position of the Fe II $\lambda$2600 line falls right at the edge of the SDSS spectra where it is not possible to measure the equivalent width.

ing of the quasars in our sample due to the intervening Mg II absorption by fitting the quasar spectra using the SDSS composite quasar spectrum (Vanden Berk et al. 2001), reddened by the Milky Way, LMC and SMC extinction curves (Gordon et al. 2003), following procedures outlined in Srianand et al. (2008, 2013) and Noterdaeme et al. (2009, 2010). We find that none of the quasars show any significant signatures of reddening, with $E(B-V)$ ranging from $-0.18$ to 0.08 and a median $E(B-V)$ of 0.02 (see Table 1). Note that the negative $E(B-V)$ values indicate that the quasar spectra are bluer than the SDSS composite spectrum. For comparison, the median $E(B-V)$ of the quasars showing H I 21-cm absorption in strong Fe II systems at $0.5 < z < 1.5$ is 0.10 (Dutta et al. 2017b).

Very Long Baseline Array (VLBA) 2.3 GHz images are available for six of the radio sources in our sample from the VLBA Calibrator Survey (VCS)[2]. We estimate the covering factor of the absorbing gas, $C_{\rm f}$, by assuming it to be the core fraction, i.e. assuming that the absorbing gas covers only the core component seen in the VLBA image. Hence, we estimate $C_{\rm f}$ from the ratio of the peak flux density in the VCS image to the total arcsecond-scale flux density at 2.3 GHz [obtained by interpolating flux densities available from the NASA extragalactic data base [3] (Gregory & Condon 1991; Condon et al. 1998)]. The $C_{\rm f}$ values are provided in Table 1.

## 3 OBSERVATIONS AND DATA REDUCTION

The observations were carried out using the L-band receiver on GMRT, with the 4 MHz baseband bandwidth split into 512 channels (spectral resolution $\sim$2 km s$^{-1}$ per channel, velocity coverage $\sim$1000 km s$^{-1}$). Data were acquired in two polarization products, XX and YY. Standard calibrators were regularly observed during the observations for flux density, bandpass, and phase calibrations. The pointing centre was at the quasar coordinates and the band was centred at the redshifted H I 21-cm line frequency. The details of the radio observations of the sources are given in Table 2. The observations of J1619+3030 were affected by strong RFI and we were not able to obtain any useful data for it.

The data were reduced using the National Radio Astronomy Observatory (NRAO) Astronomical Image Processing System (AIPS) following standard procedures as described in Gupta et al. (2010). Three of the radio sources (J0209$-$0438, J0255+0253 and J1423+5150) are extended in our GMRT continuum images (typical spatial resolution $\sim2''$), while the rest are compact. The radio continuum maps of these three extended sources overlaid on SDSS images are shown in Fig. 1. The H I 21-cm absorption spectra were extracted at the locations of the continuum peak flux density in all cases, that also coincide well (within $\sim1''$) with the optical positions of the quasars in SDSS images. We also searched for H I 21-cm absorption towards the lobes in these three cases, but did not detect any significant absorption.

## 4 RESULTS

We have detected H I 21-cm absorption in two (at $z_{\rm abs}$ = 0.3940 towards J1428+2103, and at $z_{\rm abs}$ = 0.3289 towards J1551+0713) out of 11 strong Mg II systems. Tentative absorption features were seen towards J0859+1552 and J1628+4734, and hence these sources were reobserved. However, these tentative features are at less than $2\sigma$ significance in the co-added spectra and they are not consistently produced in the individual polarization spectra. Therefore we consider these to be non-detections. The parameters estimated from the GMRT H I 21-cm absorption spectra are summarized in Table 3. In case of the extended radio sources, results from spectra extracted towards the lobes, as marked in Fig. 1, are also provided. We list the standard deviation in the optical depth at $\sim$2 km s$^{-1}$ spectral resolution ($\sigma_\tau$), and the $3\sigma$ upper limit on the integrated optical depth from spectra smoothed to 10 km s$^{-1}$ ($\int \tau dv_{10}^{3\sigma}$). In case of the detections, we provide the peak optical depth ($\tau_{\rm p}$), the total integrated optical depth ($\int \tau dv$), the velocity width which contains 90% of the total optical depth ($v_{90}$), and the velocity offset of the peak H I 21-cm optical depth from the strongest metal component in the SDSS spectrum ($v_{\rm off}$). Additionally, we estimate $N$(H I) from $\int \tau dv$ of the detections, or $3\sigma$ upper limit to it from $\int \tau dv_{10}^{3\sigma}$ in case of non-detections, assuming $T_{\rm s}$ = 100 K, typical of the CNM in the Milky Way (Wolfire et al. 1995; Heiles & Troland 2003), and covering factor, $C_{\rm f}$ = 1. We note that the small velocity widths ($v_{90}$ $\sim$ 5 and 14 km s$^{-1}$) of the two H I 21-cm absorption lines reported here support the correlation between $v_{90}$ of H I 21-cm absorption lines and redshift noted by Dutta et al. (2017b).

The H I 21-cm absorption spectra for the non-detections are shown in Fig. 2. The Gaussian fits to the two H I 21-cm absorption are shown in Fig 3. The number of Gaussian components is determined based on the fit with $\chi^2_\nu$ nearest to unity. Table 4 gives details of the Gaussian fits, i.e. $z_{\rm abs}$, full-width-at-half-maximum (FWHM) and $\tau_{\rm p}$ of individual Gaussian components. We also constrain the kinetic temperature, $T_{\rm k}$, and $N$(H I) from the FWHM and $\tau_{\rm p}$ of the Gaussian components (see section 4 of Dutta et al. 2017b).

### 4.1 H I 21-cm absorption towards J1428+2103

The H I 21-cm absorption towards J1428+2103 is best fit with two Gaussian components, A and B, with FWHM $\sim$9 km s$^{-1}$ and $\sim$5 km s$^{-1}$, respectively (see Table 4). The background radio source is compact in the 2.3 GHz VCS image. If we use the $C_{\rm f}$ obtained from this image (Table 1), and assume $T_{\rm s}$ = 100 K, as in the Milky Way CNM, then we can constrain $N$(H I) $\sim$ 8.1 $\times$ $10^{20}$ cm$^{-2}$. On the other hand, using the constraint obtained on $T_{\rm k}$ from the FWHM, and assuming that the spin temperature follows the kinetic temperature (Field 1959; Bahcall & Ekers 1969; McKee & Ostriker 1977; Wolfire et al. 1995; Liszt 2001; Roy et al. 2006), we can obtain a conservative upper limit on the $N$(H I) of the two absorption components A and B as, $N$(H I) $< 6.7 \times 10^{21}$ cm$^{-2}$ and $< 1.7 \times 10^{21}$ cm$^{-2}$, respectively. Hence, this absorption is likely to arise from a DLA. Note that the H I associated with metal line absorption from different components of the gas need not necessarily be detected in 21-cm absorption, either because it is too warm or it has low covering factor of the background radio source (e.g. Srianand et al. 2012; Rahmani et al. 2012; Dutta et al. 2015). Hence the total $N$(H I) associated with the system could be larger. No Ca II and Na I absorption from this system is seen in the SDSS spectrum of the quasar. We estimate $3\sigma$ upper limit of $W_{\rm Ca\,II} \leqslant$ 0.5 Å and $W_{\rm Na\,I} \leqslant$ 0.5 Å. We identify a possible host galaxy candidate located $\sim5''$ north of the quasar ($b \sim$ 26 kpc) in the SDSS image (Table 1), which has a consistent photometric redshift ($z_{\rm phot}$ = 0.357 $\pm$ 0.089).

[2] http://www.vlba.nrao.edu/astro/calib/
[3] https://ned.ipac.caltech.edu/

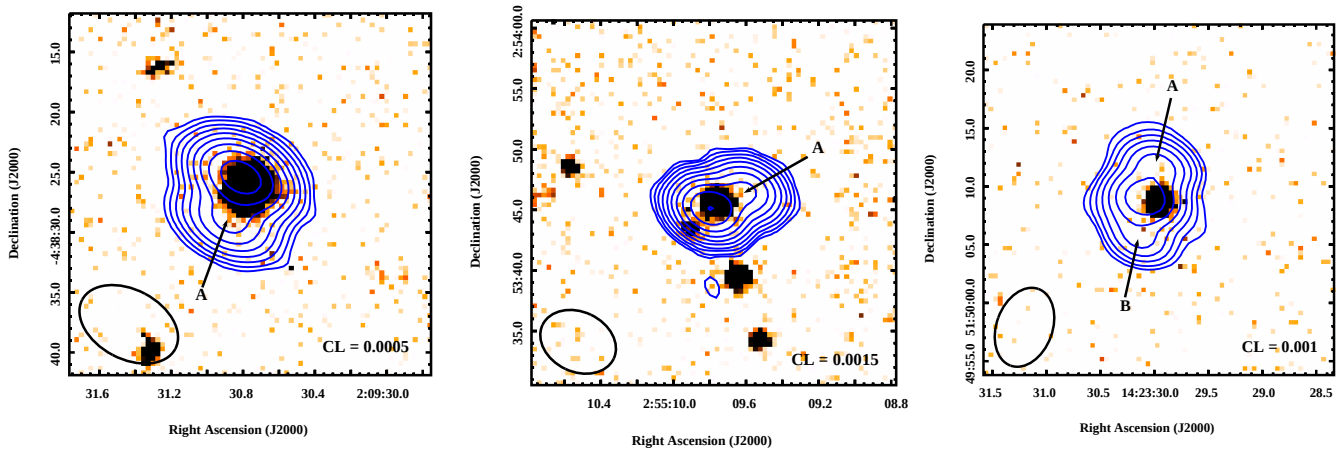


(a) J0209−0438 (b) J0255+0253 (c) J1423+5150

**Figure 1.** SDSS $r$-band images overlaid with the GMRT 1.4 GHz continuum contours of the radio sources: (a) J0209−0438, (b) J0255+0253 and (c) J1423+5150. The restoring beam of the continuum map is shown at the bottom left corner. The contour levels are plotted as CL × (−1,1,2,4,8,...) Jy beam$^{-1}$, where CL is given in the bottom right of each image. The rms in the radio images in (a), (b) and (c) are 0.0001, 0.0003 and 0.0002 Jy beam$^{-1}$, respectively. The continuum peaks of the lobes are indicated in each image.

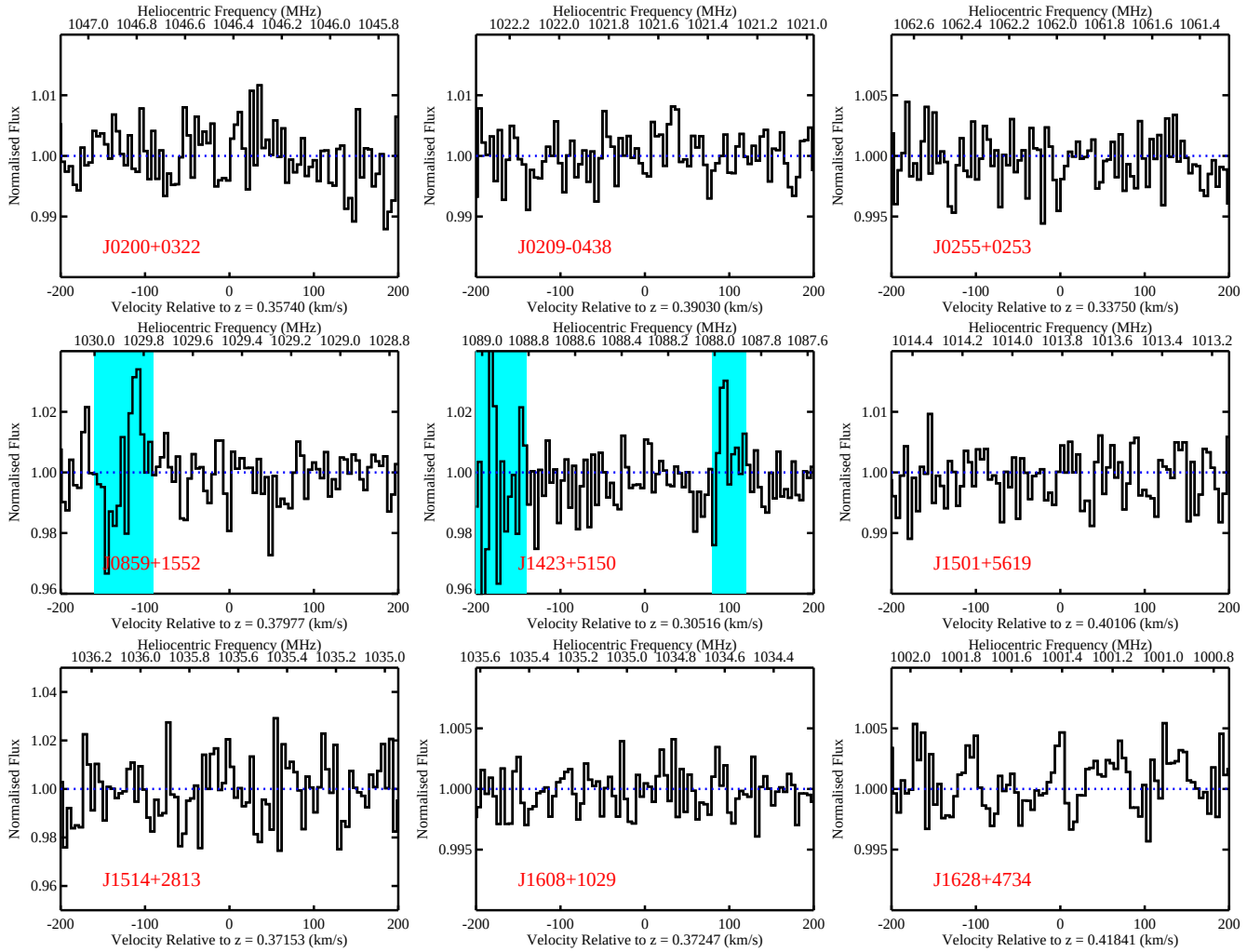


**Figure 2.** H I 21-cm absorption spectra in case of the non-detections from the sample of strong Mg II systems at $z \sim 0.35$ (smoothed to $\sim$5 km s$^{-1}$ for display purpose). The shaded regions mark frequency ranges affected by RFI. The quasar name as given in Table 1 is provided for each spectrum.

**Table 1.** Sample of strong Mg II systems at $z \sim 0.35$ toward radio-loud quasars.

| Quasar name | SDSS name | $z_{\rm em}$ | $z_{\rm abs}$ | $W_{\rm r}$(Mg II $\lambda$2796) (Å) | $W_{\rm r}$(Mg II $\lambda$2803) (Å) | $W_{\rm r}$(Mg I $\lambda$2852) (Å) | $b$ (kpc) | $E(B-V)$ | $C_{\rm f}$ |
|---|---|---|---|---|---|---|---|---|---|
| (1) | (2) | (3) | (4) | (5) | (6) | (7) | (8) | (9) | (10) |
| J0200+0322 | J020040.81+032249.4 | 1.581 | 0.3574 | $1.37 \pm 0.13$ | $0.97 \pm 0.10$ | $\leqslant$0.41 | 109 | $-0.15$ | 0.62 |
| J0209−0438 | J020930.77−043826.1 | 1.131 | 0.3903 | $1.12 \pm 0.07$ | $0.74 \pm 0.07$ | $0.40 \pm 0.06$ | 65 | $+0.05$ | 0.64 |
| J0255+0253 | J025509.76+025345.6 | 0.663 | 0.3375 | $1.32 \pm 0.20$ | $1.53 \pm 0.15$ | $0.52 \pm 0.14$ | 15 | $+0.01$ | — |
| J0859+1552 | J085943.79+155232.8 | 0.616 | 0.3798 | $1.22 \pm 0.12$ | $0.98 \pm 0.12$ | $0.38 \pm 0.09$ | 33 | $-0.06$ | — |
| J1423+5150 | J142329.98+515008.9 | 1.685 | 0.3052 | $1.14 \pm 0.33$ | $0.58 \pm 0.33$ | $\leqslant$0.74 | 98 | $+0.02$ | — |
| J1428+2103 | J142846.41+210336.6 | 1.454 | 0.3940 | $1.56 \pm 0.26$ | $1.12 \pm 0.23$ | $1.29 \pm 0.29^a$ | 26 | $-0.01$ | 0.53 |
| J1501+5619 | J150124.63+561949.7 | 1.466 | 0.4011 | $1.13 \pm 0.15$ | $1.18 \pm 0.19$ | $0.46 \pm 0.12$ | 17 | $+0.07$ | — |
| J1514+2813 | J151402.50+281334.8 | 1.548 | 0.3715 | $1.57 \pm 0.13$ | $1.35 \pm 0.13$ | $0.39 \pm 0.08$ | 46 | $+0.08$ | — |
| J1551+0713 | J155121.13+071357.7 | 0.675 | 0.3289 | $1.00 \pm 0.07$ | $1.03 \pm 0.06$ | $0.41 \pm 0.06$ | $99^b$ | $-0.11$ | — |
| J1608+1029 | J160846.20+102907.7 | 1.232 | 0.3725 | $1.27 \pm 0.11$ | $0.99 \pm 0.10$ | $\leqslant$0.44 | 57 | $+0.07$ | 0.94 |
| J1619+3030 | J161902.49+303051.6 | 1.288 | 0.3024 | $1.21 \pm 0.10$ | $1.27 \pm 0.10$ | $0.32 \pm 0.08$ | 34 | $+0.05$ | 0.48 |
| J1628+4734 | J162837.50+473410.5 | 1.632 | 0.4184 | $1.48 \pm 0.11$ | $1.43 \pm 0.11$ | $\leqslant$0.43 | 95 | $-0.18$ | 0.91 |

*Notes.* Column 1: quasar name used throughout this work. Column 2: SDSS (J2000) name of the quasar. Column 3: redshift of quasar. Column 4: redshift of intervening Mg II system. Columns 5, 6 and 7: REWs (Å) of the Mg II $\lambda$2796, Mg II $\lambda$2803 and Mg I $\lambda$2852 absorption lines, respectively, measured by us. Column 8: impact parameter (kpc) assuming that the galaxy nearest to the quasar, with consistent photometric redshift in the SDSS images, is the host galaxy. Column 9: $E(B-V)$ of the quasar from spectral energy distribution (SED) fitting, assuming that the reddening is due to the intervening Mg II absorption. Negative values indicate that the quasars are bluer than the template used. Typical systematic error in the SED-fitting method due to the dispersion of the unreddened quasar SED is ∼0.1 (Dutta et al. 2017b). Column 10: covering factor (assumed to be the core fraction) determined from 2.3 GHz VLBA image of the background radio source (see Section 2 for details).

[a] Possibly blended.

[b] Host galaxy could also be behind the foreground galaxy superimposed on the quasar in the SDSS image (see Section 4.2).

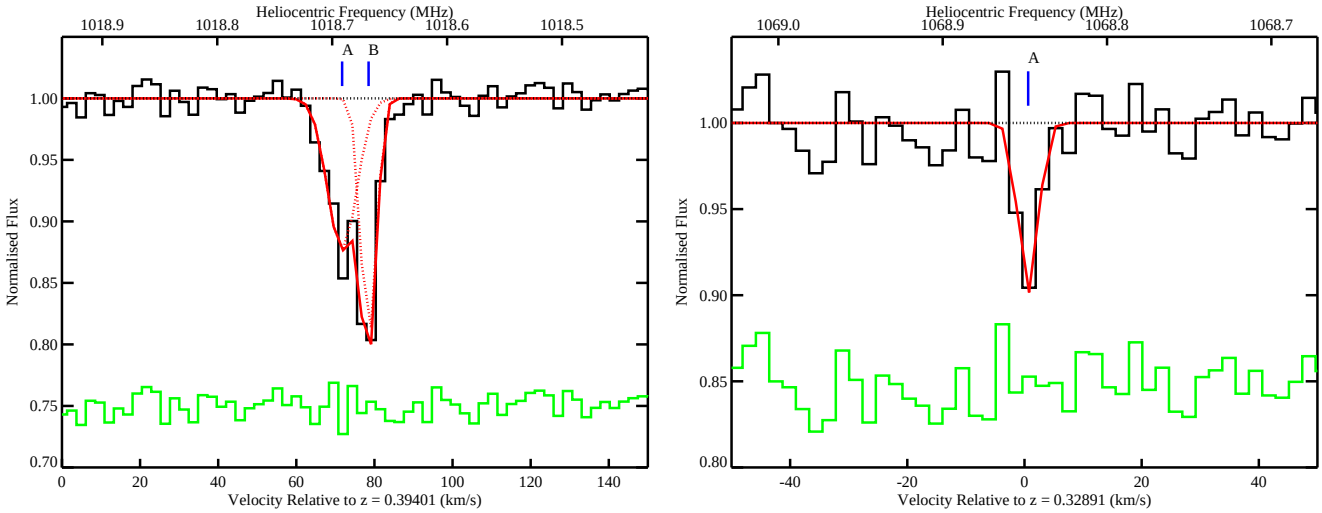


(a) J1428+2103 (b) J1551+0713

**Figure 3.** H I 21-cm absorption spectra in case of the detections: (a) J1428+2103 and (b) J1551+0713. Individual Gaussian components and the resultant fits to the absorption profiles are overplotted as dotted and continuous lines, respectively. Residuals from the fit, shifted in the y-axis by an arbitrary offset for clarity, are also shown. Locations of the peak optical depth of the individual components (as identified in Table 4) are marked by vertical ticks.

### 4.2 H I 21-cm absorption towards J1551+0713

A narrow (FWHM $\sim$4 km s$^{-1}$) H I 21-cm absorption is detected towards J1551+0713. No VLBA image of the background radio source is available. However, the radio source is compact in the ∼0.2 arcsec-scale 8.4 GHz image, with flux density of 30 mJy (Myers et al. 2003). If we assume a $C_{\rm f}$ of unity and $T_{\rm s} \approx T_{\rm k} <$ 350 K, then we can constrain the $N$(H I) as $< 3 \times 10^{20}$ cm$^{-2}$, whereas for $T_{\rm s}$ = 100 K, $N$(H I) would be $9 \times 10^{19}$ cm$^{-2}$. Hence, the H I 21-cm absorption could arise from a sub-DLA. However, as noted in Section 4.1, the total $N$(H I) associated with the Mg II system could be larger. While Ca II absorption from this system is detected in the SDSS spectrum of the quasar (see Section 2), Na I absorption is not detected ($3\sigma$ upper limit of $W_{\rm Na\,I} \leqslant 0.1$ Å). The measured $W_{\rm Ca\,II}$ is similar to that of the weak Ca II absorber population found in SDSS spectra (Wild et al. 2006; Sardane et al. 2015). Further, the ratio $W_{\rm Na\,I}/W_{\rm Ca\,II} \leqslant 0.3$ suggests that Ca is not as heavily depleted onto dust grains as expected in dense star forming regions (Welty et al. 1996).

The quasar sightline appears to pass through the outer optical disc of a foreground galaxy, i.e. $\sim$5″ north of the galaxy's centre, in the SDSS image (see fig. 5 of Dutta et al. 2017a). The redshift

**Table 2.** GMRT observation log of $z \sim 0.35$ strong Mg II systems.

| Quasar | Date | Time (h) | $\delta v$ (km s$^{-1}$) |
|---|---|---|---|
| (1) | (2) | (3) | (4) |
| J0200+0322 | 17 November 2015 | 5.7 | 2.4 |
| J0209−0438 | 8 December 2015 | 5.4 | 2.4 |
| J0255+0253 | 24 December 2015 | 0.9 | 2.4 |
| J0859+1552 | 13 November 2015 | 4.8 | 2.4 |
| | 02 October 2016 | 5.2 | 2.4 |
| J1423+5150 | 14 November 2015 | 5.3 | 2.3 |
| J1428+2103 | 5 December 2015 | 5.1 | 2.4 |
| J1501+5619 | 8 December 2015 | 2.7 | 2.4 |
| | 5 February 2016 | 2.6 | 2.4 |
| J1514+2813 | 27 December 2015 | 5.4 | 2.4 |
| J1551+0713 | 23 November 2014 | 5.3 | 2.3 |
| J1608+1029 | 9 December 2015 | 1.2 | 2.4 |
| J1619+3030 | 26 February 2016 | —RFI— | |
| J1628+4734 | 26 December 2015 | 5.3 | 2.4 |
| | 26 February 2016 | 5.0 | 2.4 |
| | 04 August 2016 | 2.6 | 2.4 |
| | 05 August 2016 | 3.8 | 2.4 |

*Notes.* Column 1: quasar name. Column 2: date of observation. Column 3: time on source in h. Column 4: channel width in km s$^{-1}$.

of this galaxy is obtained as 0.1 from South African Large Telescope (SALT) long-slit spectrum (see Appendix C of Dutta et al. 2017a). The host galaxy of the Mg II system could be located behind this foreground galaxy. However, as mentioned in Section 2, nebular emission lines at the redshift of the Mg II absorption are not detected in the SDSS quasar spectrum. Further, no extended emission at the redshift of the Mg II absorption has been detected in the SALT two-dimensional long-slit spectrum of the quasar. We also identify a possible host galaxy ($z_{\rm phot}$ = 0.355 ± 0.088) at ∼21″ north-east of the quasar ($b$ ∼100 kpc) in the SDSS images (Table 1). Deep space-based observations would help to identify the true host galaxy of this system.

### 4.3 H I 21-cm non-detections

The $\int \tau dv_{10}^{3\sigma}$ limits estimated in case of the H I 21-cm non-detections suggest that these systems would be sub-DLAs, if we assume a spin temperature of 100 K and a $C_{\rm f}$ of unity (see Table 3). Even if we assume that the gas is warmer, i.e. $T_{\rm s}$ = 1000 K, and $C_{\rm f}$ = 1, all except one of the systems with H I 21-cm non-detection would be sub-DLAs based on the $\int \tau dv_{10}^{3\sigma}$ limits. Indeed, in case of the quasar J0209−0438, a sub-DLA with $N$(H I) = $10^{19}$ cm$^{-2}$ is detected at the redshift of the Mg II system in the *Hubble Space Telescope − Cosmic Origins Spectrograph (HST−COS)* UV spectrum (Muzahid et al. 2015). Hence, we do not have sufficient sensitivity to detect absorption from cold (∼100 K) H I gas in this case. Additionally, we note that the background radio source is resolved in our GMRT image (see Fig. 1), as well as in the VCS 2.3 GHz sub-arcsecond-scale image. Using $C_{\rm f}$ estimated from this image (Table 1), the $N$(H I) measurement and $\int \tau dv_{10}^{3\sigma}$ constraint (Table 3), we estimate $T_{\rm s} > 37$ K. Further, the non-detection of $H_2$ absorption from this sub-DLA ($N(H_2) < 10^{14}$ cm$^{-2}$) by Muzahid et al. (2015), indicates that most of the gas is likely to be warm. $N$(H I) measurements for all the systems in our sample would help to interpret the H I 21-cm non-detections. Lastly, the large impact parameters of the candidate host galaxies from the quasar sightlines (based on photometric redshifts; see Table 1) could explain the lack of H I 21-cm absorption in most of the systems in our sample.

## 5 DISCUSSION

### 5.1 Detection rate of H I 21-cm absorption

We can estimate the detection rate of H I 21-cm absorption ($C_{21}$) as the fraction of systems showing H I 21-cm detections with $\int \tau dv_{10}^{3\sigma} \leqslant \tau_0$ and $\int \tau dv \geqslant \tau_0$, where $\tau_0$ is a 3$\sigma$ optical depth sensitivity. We use $\tau_0$ = 0.30 km s$^{-1}$ to estimate $C_{21}$ in this work, which corresponds to a sensitivity of $N$(H I) $\leqslant 5 \times 10^{19}$ cm$^{-2}$ for $T_{\rm s}$ = 100 K and $C_{\rm f}$ = 1, and facilitates comparisons with H I 21-cm absorption studies in the literature. We obtain $C_{21}^{\rm Mg\ II} = 0.18^{+0.24}_{-0.12}$ at $z \sim 0.35$ for our sample of strong Mg II systems. The quoted errors represent Gaussian 1$\sigma$ confidence intervals computed using tables of Gehrels (1986) assuming a Poisson distribution. We caution that due to the small sample size, the detection rate presented here has large uncertainty. The only other systematic survey of H I 21-cm absorption in Mg II-selected systems at the redshift range of our interest is presented in Lane (2000). There are four systems in the sample of Lane (2000) that satisfy our selection criteria (Section 2) [4]. Three of these systems ($z_{\rm abs}$ = 0.3939 towards 0248+430, $z_{\rm abs}$ = 0.3130 towards 1127−145, $z_{\rm abs}$ = 0.3950 towards 1229−021) show H I 21-cm absorption. The remaining system ($z_{\rm abs}$ = 0.4246 towards 0735+178) is a non-detection, however its reported optical depth limit is larger than our adopted optical depth sensitivity of $\tau_0$ = 0.30 km s$^{-1}$. Hence, combining our sample with the above systems from the sample of Lane (2000) leads to $C_{21}^{\rm Mg\ II} = 0.36^{+0.24}_{-0.15}$ at $z \sim 0.35$.

Next, from the detection rate of H I 21-cm absorption in strong Mg II systems and that of DLAs in strong Mg II systems, we can infer the detection rate of H I 21-cm absorption in DLAs. Table 1 of Rao et al. (2006) shows that the fraction of strong Mg II systems that are DLAs is $0.27^{+0.08}_{-0.06}$ at $z < 1$. If we assume that the incidence of DLAs in strong Mg II systems remains constant at $z < 1$ and consider our sample of strong Mg II systems, then the inferred incidence of H I 21-cm absorption in $z \sim 0.35$ DLAs is $C_{21}^{\rm DLA} = 0.67^{+0.33}_{-0.47}$ [note that this becomes unity when we include the systems from Lane (2000)]. This is consistent with the estimates obtained from H I 21-cm absorption studies of $z < 1$ DLAs (see Dutta et al. 2017a, and references therein), and that inferred from $0.5 < z < 1.0$ strong Mg II and Fe II systems (Gupta et al. 2012; Dutta et al. 2017b). Hence, the probability of detecting cold H I gas appears to be higher (by about four times) in DLAs compared to strong Mg II-selected systems.

From an absorption-blind survey of quasar-galaxy pairs (QGPs), Dutta et al. (2017a) have found that the detection rate of H I 21-cm absorbers is $0.16^{+0.07}_{-0.05}$ within $b \sim 35$ kpc of $z < 0.4$ galaxies. Further, the Mg II absorber-galaxy catalog of Nielsen et al. (2013) shows that the detection rate of strong Mg II absorbers at $0.3 < z < 0.5$ is $0.42^{+0.28}_{-0.18}$ when the host galaxies are within $b \sim 35$ kpc of the quasar sightlines. Hence based on the above, we expect the detection rate of H I 21-cm absorption in strong Mg II systems to be $0.38^{+0.30}_{-0.20}$ at $b \leqslant 35$ kpc. This is consistent with the H I 21 detection rate in our sample ($0.40^{+0.53}_{-0.26}$ at $b \leqslant 35$ kpc), if we assume that the nearest galaxy based on photometric redshift is the host galaxy, and that the host galaxy in case of J1551+0713 is located behind the foreground galaxy superim-

[4] Here we have not considered the $z_{\rm abs}$ = 0.4367 system towards 1243−072 (Lane & Briggs 2001; Kanekar et al. 2002). This was identified as a Mg II system by Wright et al. (1979) based on low-resolution spectrum. However, there is no published spectra or metal equivalent width information for this system.

**Table 3.** Parameters derived from redshifted H I 21-cm absorption spectra of $z \sim 0.35$ strong Mg II systems.

| Quasar | Peak Flux Density (mJy beam$^{-1}$) | Spectral rms (mJy beam$^{-1}$) | $\sigma_\tau$ | $\tau_{\rm p}$ | $\int \tau dv_{10}^{3\sigma}$ (km s$^{-1}$) | $\int \tau dv$ (km s$^{-1}$) | $N$(H I) ($T_{\rm s}$/100 K) ($1/C_{\rm f}$) ($10^{19}$ cm$^{-2}$) | $v_{90}$ (km s$^{-1}$) | $v_{\rm off}$ (km s$^{-1}$) |
|---|---|---|---|---|---|---|---|---|---|
| (1) | (2) | (3) | (4) | (5) | (6) | (7) | (8) | (9) | (10) |
| J0200+0322 | 189 | 1.3 | $\leqslant$0.007 | — | $\leqslant$0.110 | — | $\leqslant$2 | — | — |
| J0209−0438 | 202 | 1.0 | $\leqslant$0.005 | — | $\leqslant$0.096 | — | $\leqslant$2 | — | — |
| J0209−0438 | 202 | 1.0 | $\leqslant$0.005 | — | $\leqslant$0.096 | — | $\leqslant$2 | — | — |
| J0209−0438_A | 45 | 1.1 | $\leqslant$0.025 | — | $\leqslant$0.337 | — | $\leqslant$6 | — | — |
| J0255+0253 | 789 | 2.4 | $\leqslant$0.003 | — | $\leqslant$0.038 | — | $\leqslant$1 | — | — |
| J0255+0253_A | 271 | 2.3 | $\leqslant$0.009 | — | $\leqslant$0.122 | — | $\leqslant$2 | — | — |
| J0859+1552 | 115 | 1.0 | $\leqslant$0.009 | — | $\leqslant$0.130 | — | $\leqslant$2 | — | — |
| J1423+5150 | 120 | 1.3 | $\leqslant$0.011 | — | $\leqslant$0.107 | — | $\leqslant$2 | — | — |
| J1423+5150_A | 57 | 1.3 | $\leqslant$0.022 | — | $\leqslant$0.412 | — | $\leqslant$8 | — | — |
| J1423+5150_B | 32 | 1.3 | $\leqslant$0.041 | — | $\leqslant$0.735 | — | $\leqslant$13 | — | — |
| J1428+2103 | 137 | 1.3 | $\leqslant$0.010 | 0.22 | $\leqslant$0.216 | 2.36 $\pm$ 0.08 | 43 $\pm$ 2 | 14 | 71 |
| J1501+5619 | 188 | 1.1 | $\leqslant$0.006 | — | $\leqslant$0.076 | — | $\leqslant$1 | — | — |
| J1514+2813 | 57 | 1.0 | $\leqslant$0.017 | — | $\leqslant$0.289 | — | $\leqslant$5 | — | — |
| J1551+0713 | 58 | 0.8 | $\leqslant$0.014 | 0.10 | $\leqslant$0.201 | 0.48 $\pm$ 0.09 | 9 $\pm$ 2 | 5 | 0 |
| J1608+1029 | 898 | 2.1 | $\leqslant$0.002 | — | $\leqslant$0.040 | — | $\leqslant$1 | — | — |
| J1628+4734 | 330 | 0.8 | $\leqslant$0.003 | — | $\leqslant$0.060 | — | $\leqslant$1 | — | — |

*Notes.* Column 1: quasar name; in case of the extended radio sources, results from spectra extracted towards the lobes, as marked in Fig. 1, are also provided. Column 2: L-band peak flux density in mJy beam$^{-1}$. Column 3: spectral rms in mJy beam$^{-1}$. Column 4: H I 21-cm optical depth rms. Column 5: maximum H I 21-cm optical depth in case of H I 21-cm detections. Column 6: 3$\sigma$ upper limit on the integrated H I 21-cm optical depth with data smoothed to 10 km s$^{-1}$. Column 7: integrated H I 21-cm optical depth in case of H I 21-cm detections. Column 8: $N$(H I) assuming $T_{\rm s}$ = 100 K and $C_{\rm f}$ = 1, in units of $10^{19}$ cm$^{-2}$ (3$\sigma$ upper limit in case of non-detections). Column 9: velocity width which contains 90% of the total optical depth in case of H I 21-cm detections. Column 10: velocity offset of the peak H I 21-cm optical depth from the strongest metal component in the SDSS spectrum in case of detections. Note that the values given in Columns 3 and 4 are at the velocity resolution ($\sim$2 km s$^{-1}$) specified in Column 4 of Table 2.

**Table 4.** Details of the Gaussian fits to the H I 21-cm absorption lines.

| Quasar | ID | $z_{\rm abs}$ | FWHM (km s$^{-1}$) | $\tau_{\rm p}$ | $T_{\rm k}$ (K) | $N$(H I) ($T_{\rm s}$/100 K) ($1/C_{\rm f}$) ($10^{19}$ cm$^{-2}$) |
|---|---|---|---|---|---|---|
| (1) | (2) | (3) | (4) | (5) | (6) | (7) |
| J1428+2103 | A | 0.39434 | 8.6 $\pm$ 1.1 | 0.13 $\pm$ 0.03 | $<$1616 | 22 $\pm$ 9 |
| | B | 0.39438 | 4.6 $\pm$ 0.4 | 0.22 $\pm$ 0.05 | $<$462 | 19 $\pm$ 6 |
| J1551+0713 | A | 0.32891 | 4.0 $\pm$ 0.1 | 0.10 $\pm$ 0.04 | $<$350 | 8 $\pm$ 4 |

*Notes.* Column 1: quasar name. Column 2: absorption component as marked in Fig. 3. Column 3: redshift of absorption component. Column 4: FWHM (km s$^{-1}$) of Gaussian component. Column 5: peak optical depth of Gaussian component. Column 6: upper limit on $T_{\rm k}$ (K), obtained assuming the line width is purely due to thermal motions. Column 7: $N$(H I) assuming $T_{\rm s}$ = 100 K and $C_{\rm f}$ = 1, in units of $10^{19}$ cm$^{-2}$.

posed on the quasar (see Table 1). Hence, broadly we can conclude that $\sim$40% of the H I gas within $b \sim 35$ kpc of low-$z$ galaxies will produce strong Mg II absorption, and $\sim$40% of these strong Mg II absorbers will produce detectable H I 21-cm absorption. This picture is consistent with the detection rates of H I 21-cm absorption in QGPs and our sample of strong Mg II systems.

### 5.2 Redshift evolution of H I 21-cm absorbers

To study the redshift evolution of H I 21-cm absorbers in strong Mg II-selected systems, we consider our present sample and the samples of Lane (2000), Kanekar et al. (2009), Gupta et al. (2009) and Gupta et al. (2012), for which both the H I 21-cm detections and non-detections have been systematically reported, since the inclusion of individually reported detections from the literature can bias the detection rate estimates. We compare $C_{21}^{\rm Mg\ II}$ (for $\tau_0$ = 0.3 km s$^{-1}$) over $0.3 < z < 1.5$ in the left panel of Fig. 4. We show in open symbols the detection rates considering only our sample and that of Gupta et al. (2009) and Gupta et al. (2012), which are homogeneous in terms of sample selection, and treatment of optical and radio data. The detection rates upon adding the systems from Lane (2000) and Kanekar et al. (2009) are shown in filled symbols. It can be seen that due to the large uncertainties, it is difficult to interpret the redshift evolution of $C_{21}^{\rm Mg\ II}$. Considering only our measurements, the incidence of H I 21-cm absorption in strong Mg II systems does not appear to be evolving significantly over $0.3 < z < 1.5$, within the uncertainties. If the measurements of Lane (2000) are considered, there is an indication that the incidence of H I 21-cm absorption in strong Mg II systems may have increased from $0.5 < z < 1.5$ to $0.3 < z < 0.5$ by a factor of three, though the evolution is not statistically significant. Note that due to lack of low-frequency VLBA images for all the radio sources in our sample, we do not correct the measurements for $C_{\rm f}$. The detection rates for different Mg II samples at $0.5 < z < 1.5$ when corrected for partial coverage are listed in table 5 of Gupta et al. (2012).

Next, as described in Gupta et al. (2009, 2012), we can estimate the number density per unit redshift of H I 21-cm absorbers ($n_{21}$) with $\int \tau dv \geqslant \tau_0$ and $W_{\rm Mg\ II} \geqslant 1.0$ Å, from $C_{21}^{\rm Mg\ II}$ and the number density per unit redshift of Mg II absorbers ($n_{\rm Mg\ II}$) with

$W_{\rm Mg\,II} \geqslant 1.0$ Å [5]. We obtain $n_{21} = 0.02^{+0.04}_{-0.01}$ at $z = 0.35$ considering only our sample, and $n_{21} = 0.04^{+0.03}_{-0.02}$ upon including the systems from Lane (2000) (see Section 5.1). This is consistent, within the uncertainties, with the estimate of $n_{21}$ at $z = 0.1$ obtained from the detection rate of H I 21-cm absorption in low-$z$ QGPs, assuming a characteristic radius of 35 kpc (see Dutta et al. 2017a). Similar to $C_{21}^{\rm Mg\,II}$, within the large uncertainties we observe no significant evolution of $n_{21}$ over $0.3 < z < 1.5$ (see right panel of Fig. 4). The $n_{21}$ estimates are also consistent with a non-evolving population (i.e. no intrinsic redshift evolution in physical parameters for the assumed cosmology) of H I 21-cm absorbers.

## 6 SUMMARY

We have presented here the results from our GMRT search for H I 21-cm absorption in eleven strong Mg II systems at $0.3 < z < 0.5$ selected from SDSS. The main results from our study are the following:

(i) We report two new H I 21-cm absorption detections. The FWHM of the absorption lines at $z_{\rm abs} = 0.3940$ towards J1428+2103 and at $z_{\rm abs} = 0.3289$ towards J1551+0713, indicate that the gas kinetic temperature (and hence the spin temperature) is <1600 K and <350 K, respectively. The small velocity widths are also consistent with the correlation found between $v_{90}$ and $z_{\rm abs}$ by Dutta et al. (2017b).

(ii) The lack of H I 21-cm detection in the other nine Mg II systems could be because they are arising from sub-DLAs, from which we do not have sufficient optical depth sensitivity to detect cold ∼100 K gas. This is indeed the case for the system towards J0209−0438, where $N$(H I) measurement from *HST* spectra is available.

(iii) The non-detection of H I 21-cm absorption is also consistent with most of the systems having candidate host galaxies with $b > 35$ kpc, where there has been no detection of H I 21-cm absorption around $z < 0.4$ galaxies (see Curran et al. 2016; Dutta et al. 2017a). This reinforces the argument that just $W_{\rm Mg\,II} \geqslant 1$ Å selects a wide range of impact parameters, and hence additional constraints like $W_{\rm Fe\,II} \geqslant 1$ Å are required to probe high $N$(H I) cold gas at small impact parameters from galaxies (Dutta et al. 2017b). UV spectra covering Lyman-$\alpha$ and Fe II absorption from the Mg II systems would help to interpret the incidence of H I 21-cm absorption at these redshifts.

(iv) By comparing with H I 21-cm studies in samples of $0.5 < z < 1.5$ strong Mg II systems from the literature (as compiled in Gupta et al. 2012), we do not find any significant evolution in the incidence and number density per unit redshift of H I 21-cm absorbers in strong Mg II systems over $0.3 < z < 1.5$, within the uncertainties. Upcoming blind H I 21-cm surveys with the Square Kilometre Array pre-cursors are expected to provide accurate and uniform measurement of the redshift evolution of the cold gas fraction in galaxies upto $z \sim 1.5$.

## ACKNOWLEDGEMENTS

We thank the referee, Dr. Wendy Lane, for her useful comments. We thank the staff at GMRT for their help during the observations. GMRT is run by the National Centre for Radio Astrophysics of the Tata Institute of Fundamental Research. RS and NG acknowledge the support from Indo-Fench centre for the promotion of Advanced Research (IFCPAR) under Project No. 5504-2. This research has made use of the NASA/IPAC Extragalactic Database (NED) which is operated by the Jet Propulsion Laboratory, California Institute of Technology, under contract with the National Aeronautics and Space Administration.

Funding for SDSS-III has been provided by the Alfred P. Sloan Foundation, the Participating Institutions, the National Science Foundation, and the U.S. Department of Energy Office of Science. The SDSS-III web site is http://www.sdss3.org/. SDSS-III is managed by the Astrophysical Research Consortium for the Participating Institutions of the SDSS-III Collaboration including the University of Arizona, the Brazilian Participation Group, Brookhaven National Laboratory, Carnegie Mellon University, University of Florida, the French Participation Group, the German Participation Group, Harvard University, the Instituto de Astrofisica de Canarias, the Michigan State/Notre Dame/JINA Participation Group, Johns Hopkins University, Lawrence Berkeley National Laboratory, Max Planck Institute for Astrophysics, Max Planck Institute for Extraterrestrial Physics, New Mexico State University, New York University, Ohio State University, Pennsylvania State University, University of Portsmouth, Princeton University, the Spanish Participation Group, University of Tokyo, University of Utah, Vanderbilt University, University of Virginia, University of Washington, and Yale University.

[5] $n_{\rm Mg\,II}(W_0, z) = n_0 \times (1+z)^{\gamma}$, where $n_0 = 0.080\ ^{+0.015}_{-0.005}$ and $\gamma = 1.40 \pm 0.16$ for $W_0 > 1$ Å (Prochter et al. 2006).

## REFERENCES

Alam S., et al., 2015, ApJS, 219, 12
Bahcall J. N., Ekers R. D., 1969, ApJ, 157, 1055
Bergeron J., 1986, A&A, 155, L8
Bergeron J., Boissé P., 1991, A&A, 243, 344
Borthakur S., 2016, ApJ, 829, 128
Borthakur S., Tripp T. M., Yun M. S., Bowen D. V., Meiring J. D., York D. G., Momjian E., 2011, ApJ, 727, 52
Bowen D. V., Chelouche D., 2011, ApJ, 727, 47
Briggs F. H., Wolfe A. M., 1983, ApJ, 268, 76
Carilli C. L., van Gorkom J. H., 1992, ApJ, 399, 373
Chen H.-W., Helsby J. E., Gauthier J.-R., Shectman S. A., Thompson I. B., Tinker J. L., 2010, ApJ, 714, 1521
Chen S.-F. S., et al., 2016, preprint, (arXiv:1612.02829)
Churchill C. W., Kacprzak G. G., Steidel C. C., 2005, in Williams P., Shu C.-G., Menard B., eds, IAU Colloq. 199: Probing Galaxies through Quasar Absorption Lines. pp 24–41 (arXiv:astro-ph/0504392), doi:10.1017/S1743921305002401
Condon J. J., Cotton W. D., Greisen E. W., Yin Q. F., Perley R. A., Taylor G. B., Broderick J. J., 1998, AJ, 115, 1693
Curran S. J., Murphy M. T., Pihlström Y. M., Webb J. K., Purcell C. R., 2005, MNRAS, 356, 1509
Curran S. J., Tzanavaris P., Darling J. K., Whiting M. T., Webb J. K., Bignell C., Athreya R., Murphy M. T., 2010, MNRAS, 402, 35
Curran S. J., Reeves S. N., Allison J. R., Sadler E. M., 2016, MNRAS, 459, 4136
Dutta R., Srianand R., Muzahid S., Gupta N., Momjian E., Charlton J., 2015, MNRAS, 448, 3718
Dutta R., Gupta N., Srianand R., O'Meara J. M., 2016, MNRAS, 456, 4209
Dutta R., Srianand R., Gupta N., Momjian E., Noterdaeme P., Petitjean P., Rahmani H., 2017a, MNRAS, 465, 588
Dutta R., Srianand R., Gupta N., Joshi R., Petitjean P., Noterdaeme P., Ge J., Krogager J.-K., 2017b, MNRAS, 465, 4249
Field G. B., 1959, ApJ, 129, 536
Gehrels N., 1986, ApJ, 303, 336
Gordon K. D., Clayton G. C., Misselt K. A., Landolt A. U., Wolff M. J., 2003, ApJ, 594, 279

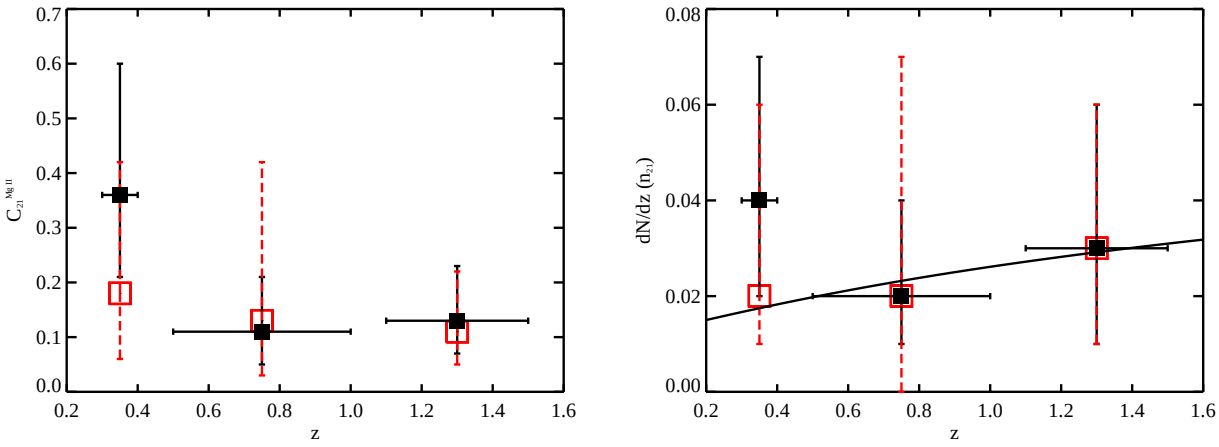


**Figure 4.** Redshift evolution of detection rate (for $\tau_0 = 0.3\,\mathrm{km\,s^{-1}}$; left) and number density per unit redshift (right) of H I 21-cm absorbers in strong Mg II systems. The open symbols (and dashed error bars) correspond to estimates based on our sample and that of Gupta et al. (2009) and Gupta et al. (2012). The filled symbols correspond to estimates upon adding the systems from Lane (2000) and Kanekar et al. (2009). The solid line is the curve for non-evolving population of H I 21-cm absorbers normalized at $z = 1.3$.


Gregory P. C., Condon J. J., 1991, ApJS, 75, 1011
Guillemin P., Bergeron J., 1997, A&A, 328, 499
Gupta N., Srianand R., Petitjean P., Khare P., Saikia D. J., York D. G., 2007, ApJ, 654, L111
Gupta N., Srianand R., Petitjean P., Noterdaeme P., Saikia D. J., 2009, MNRAS, 398, 201
Gupta N., Srianand R., Bowen D. V., York D. G., Wadadekar Y., 2010, MNRAS, 408, 849
Gupta N., Srianand R., Petitjean P., Bergeron J., Noterdaeme P., Muzahid S., 2012, A&A, 544, A21
Gupta N., Srianand R., Noterdaeme P., Petitjean P., Muzahid S., 2013, A&A, 558, A84
Heiles C., Troland T. H., 2003, ApJ, 586, 1067
Kanekar N., Chengalur J. N., 2003, A&A, 399, 857
Kanekar N., Athreya R. M., Chengalur J. N., 2002, A&A, 382, 838
Kanekar N., Prochaska J. X., Ellison S. L., Chengalur J. N., 2009, MNRAS, 396, 385
Kanekar N., et al., 2014, MNRAS, 438, 2131
Kewley L. J., Geller M. J., Jansen R. A., 2004, AJ, 127, 2002
Kulkarni S. R., Heiles C., 1988, Neutral hydrogen and the diffuse interstellar medium. pp 95–153
Lane W. M., 2000, PhD thesis, University of Groningen
Lane W. M., Briggs F. H., 2001, ApJ, 561, L27
Lanzetta K. M., Bowen D., 1990, ApJ, 357, 321
Liszt H., 2001, A&A, 371, 698
Madau P., Dickinson M., 2014, ARA&A, 52, 415
McKee C. F., Ostriker J. P., 1977, ApJ, 218, 148
Ménard B., Wild V., Nestor D., Quider A., Zibetti S., Rao S., Turnshek D., 2011, MNRAS, 417, 801
Muzahid S., Srianand R., Charlton J., 2015, MNRAS, 448, 2840
Myers S. T., et al., 2003, MNRAS, 341, 1
Neeleman M., Prochaska J. X., Ribaudo J., Lehner N., Howk J. C., Rafelski M., Kanekar N., 2016, ApJ, 818, 113
Nestor D. B., Turnshek D. A., Rao S. M., 2005, ApJ, 628, 637
Nielsen N. M., Churchill C. W., Kacprzak G. G., Murphy M. T., 2013, ApJ, 776, 114
Noterdaeme P., Ledoux C., Petitjean P., Srianand R., 2008, A&A, 481, 327
Noterdaeme P., Ledoux C., Srianand R., Petitjean P., Lopez S., 2009, A&A, 503, 765
Noterdaeme P., Srianand R., Mohan V., 2010, MNRAS, 403, 906
Prochter G. E., Prochaska J. X., Burles S. M., 2006, ApJ, 639, 766
Quider A. M., Nestor D. B., Turnshek D. A., Rao S. M., Monier E. M., Weyant A. N., Busche J. R., 2011, AJ, 141, 137
Rahmani H., Srianand R., Gupta N., Petitjean P., Noterdaeme P., Vásquez D. A., 2012, MNRAS, 425, 556
Rao S. M., Turnshek D. A., Nestor D. B., 2006, ApJ, 636, 610
Rao S. M., Belfort-Mihalyi M., Turnshek D. A., Monier E. M., Nestor D. B., Quider A., 2011, MNRAS, 416, 1215
Reeves S. N., Sadler E. M., Allison J. R., Koribalski B. S., Curran S. J., Pracy M. B., 2015, MNRAS, 450, 926
Reeves S. N., et al., 2016, MNRAS, 457, 2613
Roy N., Chengalur J. N., Srianand R., 2006, MNRAS, 365, L1
Sardane G. M., Turnshek D. A., Rao S. M., 2015, MNRAS, 452, 3192
Srianand R., Gupta N., Petitjean P., Noterdaeme P., Saikia D. J., 2008, MNRAS, 391, L69
Srianand R., Gupta N., Petitjean P., Noterdaeme P., Ledoux C., Salter C. J., Saikia D. J., 2012, MNRAS, 421, 651
Srianand R., Gupta N., Rahmani H., Momjian E., Petitjean P., Noterdaeme P., 2013, MNRAS, 428, 2198
Steidel C. C., 1995, in Meylan G., ed., QSO Absorption Lines. p. 139 (arXiv:astro-ph/9509098)
Straka L. A., Whichard Z. L., Kulkarni V. P., Bishof M., Bowen D., Khare P., York D. G., 2013, MNRAS, 436, 3200
Vanden Berk D. E., et al., 2001, AJ, 122, 549
Welty D. E., Morton D. C., Hobbs L. M., 1996, ApJS, 106, 533
White R. L., Becker R. H., Helfand D. J., Gregg M. D., 1997, ApJ, 475, 479
Wild V., Hewett P. C., Pettini M., 2006, MNRAS, 367, 211
Wolfe A. M., Gawiser E., Prochaska J. X., 2005, ARA&A, 43, 861
Wolfire M. G., Hollenbach D., McKee C. F., Tielens A. G. G. M., Bakes E. L. O., 1995, ApJ, 443, 152
Wright A. E., Peterson B. A., Jauncey D. L., Condon J. J., 1979, ApJ, 229, 73
York D. G., et al., 2000, AJ, 120, 1579
York D. G., et al., 2012, MNRAS, 423, 3692
Zhu G., Ménard B., 2013, ApJ, 770, 130
Zwaan M. A., Liske J., Péroux C., Murphy M. T., Bouché N., Curran S. J., Biggs A. D., 2015, MNRAS, 453, 1268


This paper has been typeset from a TEX/LATEX file prepared by the author.